Subanesthetic ketamine administration decreases deviance detection responses at the cellular, populational and mesoscale connectivity levels

Maria Isabel Carreño-Muñoz[1,2,*,#], Alessandra Ciancone Chama[1,2, ,*], Pegah Chehrazi[1,2], Bidisha Chattopadhyaya[2], Graziella Di Cristo[1,2,#]

Affiliations:

[1] Neurosciences Department, Université de Montréal;

[2] Centre de Recherche, CHU Sainte-Justine (CHUSJ) ;

* Equal contribution

Corresponding authors:

Maria Isabel Carreño-Muñoz

Department of Neurosciences, Université de Montréal,

Centre de Recherche Azrieli, CHU Sainte-Justine,

3175, Côte-Sainte-Catherine, Montréal, QC H3T 1C5, Canada.

E-mail: maria.munoz.hsj@ssss.gouv.qc.ca

Graziella Di Cristo,

Department of Neurosciences, Université de Montréal,

Centre de Recherche, CHU Sainte-Justine,

3175, Côte-Sainte-Catherine, Montréal, QC H3T 1C5, Canada.

E-mail: graziella.di.cristo@umontreal.ca

ABSTRACT

In the neocortex, neuronal processing of sensory events is significantly influenced by context. For instance, responses in sensory cortices are suppressed to repetitive stimuli, a phenomenon termed stimulus-specific adaptation. However, in a context in which that same stimulus is novel, or deviates from expectations, neuronal responses are enhanced. Mismatch negativity (MMN), the electroencephalography waveform reflecting rule violations, is a well-established biomarker for auditory deviant detection. MMN has been shown to depend on intact NMDA receptor signaling across species; nevertheless, the underlying mechanisms are still not completely elucidated at the neural and mesoscale levels. Using multi-electrode array recordings in awake mice, we identified a specific biphasic spiking response in a subpopulation of A1 neurons elicited by deviant, but not standard, sounds, whereby the second peak is abolished by acute subanesthetic injection of ketamine, a partial non-competitive NMDA receptor antagonist. We further showed that the posterior parietal cortex, a critical hub for multisensory integration and sensorimotor coordination, responds to unexpected and deviant, but not repetitive, sounds, and this response is dependent upon intact NMDA receptor-mediated signaling. Finally, to explore the effects of ketamine on inter-cortical communication during deviance detection, we performed Granger Causality and Weighted Phase Lag Index (WPLI) analyses during the presentation of deviant and standard sounds. This analysis showed a unidirectional functional connectivity from A1 to PPC during deviant detection, which is impaired by subanesthetic ketamine administration. By investigating how ketamine modulates neural and inter-regional communication, our findings provide novel insights into the NMDA receptor-dependent mechanisms underlying the processing of novelty and regularity in auditory stimuli.

INTRODUCTION

Animal survival critically depends on the continuous updating of sensory information and rapid processing that enables behavior. To interact efficiently with ever-changing environments, mammalian brains must continuously align incoming sensory information with predictions based on current actions or intentions. Consequently, the brain has evolved various strategies to minimize computational demands while still efficiently navigating through a constant flow of information. One such strategy is the ability to suppress responses to predictable stimuli — a phenomenon referred here as habituation — while remaining alert to unexpected changes – known as deviance detection. In sensory cortices, neurons gradually reduce their firing to repetitive sounds but preserve robust responses to rare, deviant stimuli [1]. This form of neuronal adaptation manifests in changes in event-related potentials (ERPs), time-locked brain responses that represent changes at the population level on recorded local field potentials (LFP). As it is the case for neuronal firing, repetitive sounds also elicit a progressive reduction of ERP amplitude [2], while unexpected sounds trigger a specific wave shape response known as mismatch negativity (MMN) [3], reflecting the brain's detection of deviations from auditory regularities. Together, auditory habituation and MMN both at the cellular and population level, provide a hierarchical framework for understanding how local neuronal response and large-scale network dynamics contribute to efficient sensory monitoring and predictive coding in the brain.

At the inter-cortical connectivity (mesoscale) level, recent studies have proposed that both functional and anatomical connectivity between distinct brain regions are essential for processing standard and deviant auditory stimuli. While several studies have emphasized the role of frontal cortex in top-down modulation of sound predictability [4], emerging evidence also highlights the potential involvement of the posterior parietal cortex (PPC), a higher-order associative region involved in both multisensory integration and sensorimotor coordination [5,6]. Studies in rodents and humans have shown that the PPC exhibits robust responses to unexpected stimuli in the auditory domain [7,8]. Further, at the cellular level, PPC neurons can discriminate the presence or absence of expected auditory stimuli, in awake mice [9]. However, at the mesoscale connectivity level, the specific role of the PPC in discriminating redundant from deviant stimuli in the auditory modality remains unclear.

Although the synaptic mechanisms underlying deviant detection are not completely understood yet, most studies propose N-methyl-D-aspartate (NMDA) receptors activity as a central mechanism [10,11]. For example, studies using pharmacological NMDA receptor antagonists, such as ketamine, a partial non-competitive antagonist, reliably reported reductions in MMN amplitude and auditory habituation in humans[10,12,13], with smaller MMN amplitudes specifically associated with the emergence of more pronounced schizophrenia-like negative symptoms in healthy volunteers[14,15] Whereas the effects of ketamine administration on MMN and auditory habituation at the local population level are relatively well documented, the impact of ketamine at the neuronal and mesoscale levels, particularly in relation to functional inter-cortical connectivity and network dynamics, remains largely unexplored.

In this study, using multi-electrode array recordings, we assessed how a subanesthetic dose of ketamine affects auditory deviance detection and habituation at the population level, through ERP-MMN waveforms and evoked oscillatory activity analysis, and at the neuronal level, by analyzing single-unit firing, in the primary auditory cortex (A1). Furthermore, we explored the functional connectivity between PPC and A1 to gain a deeper understanding of the broader network dynamics involved in auditory deviance detection and habituation.

MATERIAL AND METHODS

Animals

Experimental procedures involving mice were approved by the "Comité Institutionnel de Bonnes Pratiques Animales en Recherche" (CIBPAR) of the Research Center of Sainte-Justine Hospital in accordance with the principles published by the Canadian Council on Animal Care. Six adult C57Bl/6 mice (four males and two females) were used in this study. Mice were implanted at postnatal day (P)70–90 and recorded between P80 and P200. All animals were housed with two to five mice/cage from weaning until surgery, after which they were housed singularly for the duration of the experiment. Animals were kept on a 12h/12h light/dark cycle and provided with nesting material, food, and water *ad libitum*. All experiments were performed during the light period under constant mild luminosity (60 lx).

We checked and noted the exact stage of the females' estrous cycle after each recording session by histological inspection of a vaginal smear[16]. To avoid variability and the concomitant effect of sex hormones, the two females included in our analysis were in the diestrus phase in all conditions (control, vehicle and ketamine).

Surgery

Cranial surgery was performed under deep anaesthesia, induced by an intraperitoneal injection of ketamine/xylazine cocktail. Body temperature was maintained at 37°C using a feedback-controlled heating pad. Mouse heads were fixed in a stereotaxic frame (Kopf Instruments, USA). Analgesics were given locally subcutaneously (Lidocaine 2%, Aspen Pharmacare, Canada) and an intraperitoneally dose of 30 mg/Kg (Buprenorphine, 0,3mg/ml, Vetergesic Multidose, Ceva) 5 min before incision. During the whole surgery, eyes were protected and hydrated using Opticare eye lube (CLC Medica, Canada). The skull was exposed and thoughtfully cleaned, and treated with an activator (Metabond Quick, Parkell, USA). The coordinates of the targeted areas (described below) were marked with a permanent marker before fixing the skin around the exposed skull with Vetbond tissue adhesive (3M, USA). Then a first layer of dental cement (Metabond Quick, Parkell, USA) was applied to cover the whole exposed skull except the marked coordinates. Craniotomies were then performed above the targeted areas.

In a first set of experiments, custom-made clusters of four to six 50 µm-diameter-insulated-tungsten wires were implanted in every targeted area. In each one of those clusters, wire tips were 50–150 µm apart. A custom-designed and 3D-printed microdrive-like scaffold held the three electrode clusters at fixed positions as we previously did in [17], thus allowing the simultaneous implantation of all three and reducing surgery time. In a second set of experiments, four independently movable tetrodes were targeting primary auditory cortex. Each tetrode was fabricated out of four 10 µm tungsten wires (H-Formvar insulation with Butyral bond coat California Fine Wire Company, Grover Beach, CA) that were twisted and then heated to bind them into a single bundle. The tips of the tetrodes were then gold-plated to reduce the impedance to 200-400 kΩ. The use of tetrodes provides not only local field potential (LFP) recordings but also high-density spiking activity, allowing for the

characterization of single-unit discharges. In this case the 3D printed microdrives was manufactured by axona.

A ground-and-reference wire was also gently introduced in the contralateral frontal lobe. The microdrive apparatus and the ground-and-reference wire were then daubed with dental acrylic (Ortho-Jet Powder and Jet liquid, Lang Dental, USA) to encase the electrode-microdrive assembly and anchor it to the skull. When implanting tetrodes, a drop of silicone elastomer (WPI, USA) was applied around the tetrodes before the acrylic to let tetrodes free of movement. For 1 week after surgery, animals were treated with Metacam and the skin around the implant was disinfected daily.

Coordinates

Electrode clusters were implanted at the following coordinates: primary auditory cortex (A1), −2.5 mm posterior to bregma, 3.9 mm lateral to the midline and 0.8 mm deep; primary visual cortex (V1), −4 mm posterior to bregma and 2 mm lateral to the midline; posterior parietal cortex (PPC), −2 mm posterior to bregma and 1.7 mm lateral to the midline. Clusters placed in the V1 and PPC targeted both the supra and infragranular layers; those placed in the A1 targeted layer 5. Data shown here are only signal from layer 5 A1 and PPC.

EEG data acquisition

EEG recordings were performed using an open-ephys GUI platform (https://open-ephys.org/). Data were acquired at 20 KHz with a custom-made headstage using Intan Technologies' RHD Electrophysiology Amplifier chip. Custom designed auditory and visual trigger generator devices sent triggers directly to the recording system, assuring the time precision of the stimuli presentation. Starting 1 week after surgery, animals were habituated daily for 4 days to an open field (15–20 min each time), before being recorded during auditory stimulation protocols from Day 5. We used a dimly illuminated open field environment (45 × 35 cm), surrounded by 60 cm-high transparent walls and equipped with video monitoring. The walls were sprayed and wiped clean with Peroxigard (Virox Technologies) 15 min before the introduction of each animal. Two speakers were placed ∼10 cm from the walls of the open field. Baseline activity was recorded at the beginning of each session for a period of 10

min, while mice were freely exploring the open field. EEG recordings during auditory stimulations were conducted for 20–30 min, a total of six to ten times, on alternate days.

Auditory stimulations protocols

All stimulations were presented at an intensity of 70-75 dB. The oddball paradigm consisted in a sequence of five to nine repetitive (standard) sounds - at 5 kHz - followed by a deviant sound - at 10 kHz. Sequences were presented in a pre-established pseudorandom order. Sounds lasted 50 ms and were presented with a 1 s interstimulus interval. The full protocol lasted 10 min. Pure tone stimulation paradigm, consisted in a series of 500-ms long 5 and 10 kHz pure tones presented with a random interstimulus interval of 2 to 5 s. Each pure tone was presented 60 times using a random order. The full protocol lasted 5 min.

EEG preprocessing

EEG signals were downsampled to 2000 Hz and a passband filter (0.5–150 Hz) was applied. A notch filter (59.5–60.5 Hz) was also applied to remove residual 60 Hz power-line noise contamination. Data were then segmented into periods of different lengths, depending on the stimulation protocol: 1400 ms (500 ms pre- and 900 ms post-stimulus onset) for the auditory oddball protocol and 2500 ms (1000 ms pre- and 1500 ms post-stimulus onset) for the pure tone stimulation. Trials containing per sample segments with an intra-channel average higher than four times the total trial standard deviation (SD) were tagged, visually inspected and removed. Only sessions containing more than 50 clean trials were kept for further analyses.

Data analysis

None of the recorded animals were excluded from the final analysis. Signal analysis and quantification was performed using custom MATLAB (The Mathworks Inc.) codes, available upon request.

Evoked Related Potentials. The EEG signal was baseline corrected to the mean voltage of the 100 ms prior to stimulus onset and averaged over trials. Event-related potential components baseline-to-peak N1 and absolute P1 were analysed from the evoked related potentials (ERPs). The N1 amplitude was automatically detected by subtracting the minimum voltage (negative peak) within a 10- to 80-ms time window after stimulus onset to the averaged baseline value. The P1 amplitude was calculated by measuring the maximum

voltage (positive peak) within an 80- to 150-ms time window after stimulus onset to the average baseline value. Analyses were carried out using Fieldtrip toolbox[18]. To quantify habituation from ERPs, we calculated the ratio between the N1 amplitudes of the first (S1) and the second (S2) standard sounds by dividing S2 by S1. These ratios were then converted to a logarithmic base 10 scale and multiplied by 10, using the following formula:

$$10 * log10(\frac{S2}{S1})$$

Mismatch negativity (MMN) trace was calculated by subtracting the EEG trace of the standard sound (S1) from the EEG trace of the deviant sound (D). The pattern obtained was then used to detect N1 (MMN-N1) and P1 (MMN-P1) amplitudes from each subject ERPs.

Power spectral density. Baseline power spectral density (PSD) analysis, where done during periods of immobility during the first 10 minutes of the recording session when no auditory stimulation was taking place. Immobility periods were defined by establishing a velocity threshold of the animal body center at <1 cm/s for at least 2 seconds. To estimate the power spectrum using Fast Fourier Transform (FFT), we used the Welsh method implemented in Matlab. The estimated power spectrum was normalized by the total power of the signal and plotted using logarithmic scale for visualization purposes.

Evoked PSD analysis was performed on the 300 ms following stimulation and baseline corrected using a similar formula than before:

$$10 * log10(\frac{FFT\ Baseline}{FFT\ Stimulation})$$

To adopt an approach comparable to the MMN trace and facilitate the comparison of habituation and deviant detection between experimental groups, we calculated the difference (Δ) in evoked PSD by subtracting the corresponding sound conditions: D − S1 (deviant detection) and S2 − S1 (habituation).

Spiking activity analysis. Offline processing of electrophysiological data began with the extraction of spikes from the high-pass filtered signal (800–5000 Hz) of recordings sampled at 20 kHz. Action potentials exceeding 5 standard deviations above the baseline mean were detected. Spike waveforms were then characterized by feature extraction, and putative neuronal units were identified using principal component analysis followed by automatic clustering using klustakwik[19] (http://klustakwik.sourceforge.net/). Identified clusters were manually refined with a graphical cluster-cutting program[20]. Only units exhibiting a clear refractory period (<2 ms) in their auto-correlograms and well-isolated cluster boundaries were included in subsequent analyses.

Peri-stimulus time histograms (PSTH) were performed using the mlib toolbox by Maik Stüttgen (https://de.mathworks.com/matlabcentral/fileexchange/37339-mlib-toolbox-for-analyzing-spike-data). PSTH were used to calculate the spike density function (SPF) using the same mlib toolbox. Each neuron SPF was baseline corrected by subtracting SPF values during 50 ms before the stimulus presentation to the whole SDF. Then, we identified 3 types of neurons: responding-excited, responding-inhibited and non- responding neurons depending on whether their firing rate increased, decreased or remained unperturbed after stimulus presentation respectively.

As we did for the PSD analysis, to adopt an approach comparable to the MMN trace and facilitate the comparison of habituation and deviant detection between experimental groups, we calculated the difference (Δ) SDF by subtracting individual neurons SDF following deviant sound from SDF following standard sounds.

Connectivity analysis. Granger causality and Weighted Phase Lag Index (WPLI) analysis between A1 and PPC were performed using fieldtrip toolbox[18]. Both analyses were performed during the MMN response period (80-320 ms after the stimulus presentation) to avoid the first abrupt N1 peak and therefore the non-stationarity of the EEG signal. Both, Granger causality and WPLI were calculated using a Fourier-based non-parametric spectral factorization approach, employing a multi-taper frequency transformation with DPSS tapers of order 5 and a padding factor of 3. As before, we calculated the difference (Δ) Granger causality and WPLI spectrograms by subtracting the spectrogram calculated during the

periods following deviant sound (D) stimulation from those following standard sound (S1) stimulations.

RESULTS

Subanesthetic ketamine administration significantly reduces MMN response and auditory habituation.

To validate previous findings reporting a reduction of MMN responses in humans[10], primates[21] and rodents[22], we first assessed the effect of an acute subanesthetic dose of ketamine (8 mg/Kg) or vehicle on auditory MMN response and habituation in freely moving mice. The dose of ketamine was selected based on previous preclinical studies showing its rapid effects on cortical activity[23]. Six animals implanted with intracranial electrodes and familiarized with an open field arena were recorded before and after ketamine or vehicle injection during an auditory oddball paradigm, consisting of a series of repetitive (standard) sounds randomly interrupted by deviant sounds (Figure 1A). We calculated MMN by subtracting the EEG trace of the standard sound from the EEG trace of the deviant sound. The positive deflection in this waveform, peaking approximately 100-250 ms after stimulus onset, is known as the MMN response, and it reflects the automatic brain's detection of deviations from auditory regularities. Our results show that ketamine, but not vehicle, administration significantly reduced the amplitude of MMN response, that corresponds to the P1 component (first positive peak, 100 ms after stimulus onset) of the MMN waveform (Figure 1C). This data is consistent with observation reported in previous studies in humans[10], primates[21] and rodents[22], thus validating our model. Acute ketamine administration did not induce a reduction of MMN N1 amplitude (first negative peak), as a previous study reported[24], although acute vehicle injection did significantly reduce MMN N1 amplitude (Figure 1C).

Acute ketamine injection, but not vehicle, also significantly disrupted auditory habituation to standard sounds (Figure 1F), measured as the ratio between the N1 amplitude of the first (S1) and the second (S2) standard sounds, validating previous observations in humans[25]. Since higher doses of ketamine administration can induce hyperlocomotion[25]and previous studies showed that auditory processing is modulated by motor activity [26,27], we measured the total

distance traveled by each mouse during the whole recording session. We found no effect of ketamine or vehicle injection on mouse locomotion (Figure1G), thus ruling out an effect of altered motor activity on auditory processing.

Subanesthetic ketamine administration significantly reduces the late component of spiking activity response.

To further understand the effect of ketamine on MMN responses at the cellular level, we analyzed concomitant neuronal activity during oddball protocol stimulation after vehicle or ketamine injection. To do so, we identified spiking activity of individual neurons and evaluated their firing rates by calculating their peri-stimulus time histograms (PSTH, Figure 2A, lower panels) and spike density functions (Figure 2B). Our results show two different populations: neurons that increase (excited, Figure 2A-D) and neurons that decrease (inhibited, Figure 2E-H) their firing rate immediately after the deviant sound onset, respectively. In naïve mice, deviant, but not standard, sounds induced a biphasic response in the spiking activity of A1 neurons that were excited by the sounds (Figure 2B). This response was characterized by a fast and early burst of activity peaking at 25 ms after stimulus onset, followed by a slow and late response at 100-200 ms after stimulus onset, sharing common temporal dynamics with the MMN response. This observation is in line with previous reports[28,20] suggesting that this second late component of spiking activity may code for novelty in A1 neurons [29] as well as those in other regions such as the substantia nigra[30] and PFC[31]. To facilitate the comparison between experimental groups, we calculated the difference (Δ) in spike density functions (SDF) by subtracting the standard sound condition (S1) from the deviant sound condition (D). We refer to this difference measure as Δ SDF (Figure 2C, 2G). Analysis of Δ SDF showed that ketamine, but not vehicle, administration completely abolished this novelty-related late component of the spiking activity response (Figure 2D), therefore specifically affecting the saliency of the novel stimuli but not its deviance nature within the sequence of sounds.

Conversely, neurons that were inhibited specifically by deviant sounds showed a slower and monophasic negative response that was not affected by ketamine administration (Figure 2E-H). These findings indicate that there are at least two different neuronal populations in A1

which differ in their sensitivity to ketamine. These findings indicate that stimulus-specific inhibitory responses may persist despite reduced NMDA signaling, while novelty specific excitatory responses require intact NMDA receptor function, suggesting a critical role for NMDA-mediated synaptic transmission in encoding auditory novelty.

Oscillatory activity evoked by deviant sounds is significantly reduced by subanesthetic ketamine administration.

Sensory stimulation reliably evokes a 40 Hz response in primary sensory areas across species, reflecting enhanced sensory processing during early perceptual encoding.[3,23,32,33] To investigate whether ketamine administration affects this response in A1, we evaluated the oscillatory activity following standard and deviant sound presentations. Whereas baseline oscillatory activity was similar between groups (Figure 3A-B), naive animals showed a strong response at 40 Hz evoked specifically by deviant, but not standard, sounds (Figure 3C, left). To facilitate comparing the response in the different experimental groups, we calculated the difference (Δ) in evoked PSD, (referred to as Δ PSD), by subtracting the following sound conditions: deviant minus S1 (deviant detection) and S2 minus S1 (habituation) (Figure 3D, 3E). Ketamine, but not vehicle, administration was sufficient to significantly reduce the evoked 40 Hz response in the Δ-PSD (Figure 3D, 3E). Of note, following ketamine administration the response at 40Hz evoked by standard sounds appears higher than in naïve or vehicle injected mice (Figure 3C), consistent with previous reports showing that ketamine increases the evoked responses to standard sounds[12,34]. We further evaluated habituation by comparing evoked oscillatory activity during S1 and S2. Contrary to what was observed in naïve mice or following vehicle administration (Figure 3F, left), evoked responses at 40Hz during S2 were significantly reduced following ketamine administration (Figure 3G-H). Consistent with our data, previous studies have shown that ketamine impairs evoked gamma (~40 Hz) responses to sounds presented at random inter-trial intervals [22,35]. Therefore, altogether, these results suggest that subanesthetic ketamine generally disrupts the brain's ability to respond to unpredictable stimuli in auditory input streams.

Posterior parietal cortex response to deviant sounds requires NMDA receptor-mediated signaling.

Emerging evidence suggest that the PPC, a higher-order associative region involved in both multisensory integration and sensorimotor coordination[5,6], is implicated in top-down modulation of sound predictability [4]. Therefore, we next investigated whether PPC responds to rule violation in the auditory stream. We observed that PPC robustly responds to deviant sounds, while its response to standard sounds is negligible (Figure 4A, D). To determine whether this differential responsiveness is due to the distinct nature of the sounds (5 kHz vs. 10 kHz) or their predictability, we presented these two sounds with a randomized order and inter-trial interval. Notably, when these two sounds were unexpected, PPC robustly responded to both 5 kHz and 10 kHz sounds (Supplementary figure 1), indicating that the PPC specifically responds to unexpected and deviant auditory stimuli, but not to standard sounds. Next, we analyzed MMN waves (D-S1) and observed a prominent P1 peak in naïve mice, as was the case in A1. Ketamine (Figure 4A-C), but not vehicle (Figure 4D-F), administration induced a significant reduction of the MMN P1 response in the PPC, similarly to what observed in A1. Conversely MMN N1 peak was not significantly affected by ketamine or vehicle injection (Figure 4C, F). Furthermore, neither ketamine nor vehicle administration had any significant influence on auditory habituation (Figure 4G-J), suggesting that the PPC is not involved in habituation responses to repetitive stimuli. These results indicate that PPC responses to deviant sounds require intact NMDA receptor mediated signaling.

Subanesthetic ketamine administration disrupts A1 to PPC functional connectivity elicited by auditory deviance detection.

To explore the effects of ketamine on inter-cortical communication during deviance detection, we performed Granger Causality and Weighted Phase Lag Index (WPLI) analyses during the presentation of deviant and standard sounds. Granger causality analysis quantifies the directional influence among time series by determining whether past values of one signal improve the prediction of future values of another[36]. WPLI, on the other hand, assesses the phase synchronization between signals, offering a robust measure of functional

connectivity[37]. We applied both methods during the MMN response (80-320 ms after stimuli presentation), a time window chosen to avoid erratic or sudden changes in the signal due to the non-stationary nature of the evoked potentials.

To compare the responses in the different experimental groups, we calculated the subtraction index (Δ) for deviance detection (D-S1) and habituation (S2-S1) using both analysis methods (referred to as Δ Granger and Δ WPLI in Figure 5, Supplementary figure 2, Supplementary figure 3). The analysis of Δ Granger (Figure 5, Supplementary figure 2) showed an increased connectivity between A1 and PPC at 40 Hz, specifically during deviant but not standard sounds, thus suggesting an important role of A1-PPC connectivity underlying deviance detection but not auditory habituation. Of note, this communication at 40 Hz was disrupted following ketamine, but not vehicle, administration (Figure 5A, Supplementary figure 2). Granger causality analysis further highlighted the directional nature of this communication which appeared to be exclusively from A1 to PPC, with no reciprocal influence in the opposite direction. These results on A1-PPC functional connectivity were also replicated and confirmed via WPLI analysis (Supplementary figure 3).

Overall, this data suggests that rule violation in the auditory stream elicits functional communication from A1 to PPC, which is dependent on intact NMDA-mediated signaling.

DISCUSSION

Under the predictive coding framework, the brain generates a model of the environment based on previous experiences. The auditory oddball paradigm (repeating standard and rare deviant stimuli) has been used to investigate how the brain is able to encode regular auditory patterns, generates an internal model to lower perception of regularities, and then detects deviations from these internal models[3,38]. Incoming sensory information is continuously compared against internal models, and when predictions fail, a prediction error signal emerges. MMN, the electrophysiological response to rule violations, is a well-established biomarker of auditory deviant detection, whereby an auditory evoked potential to a rare deviant stimulus is greater than that in response to repeating standard stimuli. Our findings align with previous work demonstrating that MMN depends on intact NMDA receptor

signaling across humans [10,13,39], primates [21] and rodents [22,28] , however, the underlying neural and inter-cortical network mechanisms are still under debate.

In this study, we show that the firing response of a subpopulation of A1 follows a biphasic pattern: a rapid initial peak shortly after stimulus presentation, followed by a slower, later peak (between 100ms and 250ms) that coincides with the timing of the MMN response at the population level. This biphasic pattern consistently appeared during deviant sounds, while standard sounds only elicited monophasic responses. Furthermore, sub-anesthetic ketamine administration significantly and specifically reduced the second peak of spiking activity following the presentation of a deviant sound. This data suggests that ketamine administration has a selective effect on the later, higher-order realization of sound processing. The slower, ketamine-sensitive, peak of neuronal firing could be due to disinhibition of cortical excitatory activity due to a greater NMDA sensitivity of inhibitory circuits[23,40-44]. For example, previous studies have shown that low-dose ketamine preferentially inhibit NMDA receptors containing the 2A subunit (GluN2A) in PV+ interneurons, resulting in rapid, sex-specific responses in pyramidal cell activity and gamma-band oscillations in visual cortex [23]. Decreased activity of PV+ interneurons could indeed explain our observations, as reduced evoked 40 Hz rhythms have been linked to PV+ interneuron dysfunction[23,45]. Additionally, long-range callosal PV+ neurons have been shown to play a critical role in inter-area connectivity, in different cortical regions, including the prefrontal [46] and auditory cortex[47] . Other GABAergic interneurons populations, including VIP and SST+ interneurons have been involved in disinhibitory mechanisms mediated by neuromodulators (reviewed in [48]); however, whether and how the activity of different interneuron populations is affected by acute subanesthetic ketamine treatment remain to be elucidated.

Of note, subanesthetic ketamine administration can bidirectionally modulate cortical acetylcholine levels[49,50] . Since cholinergic, and in particular, nicotinic stimulation has been demonstrated to enhance MMN amplitudes[51-56], altered basal forebrain to A1 communication could contribute to the observed ketamine effects on MMN and neuronal firing, possibly by cross-talking with dis-inhibitory microcircuits. Another complementary possibility is that this second peak of A1 neurons firing elicited by the deviant sound could be mediated by astrocytic signaling. In the lateral habenula, for example, it has been shown that stress induces

a bimodal neuronal response, similarly to what we observed in A1 neurons following deviant sounds [57]. In this region, the second peak of neuronal activation appears to be mediated by astrocytic release of the gliotransmitters glutamate and ATP/adenosine [57]. Further, a recent study has shown that neuromodulators can signal through astrocytes to modulate synapse strength in adult mouse hippocampus[58] . Whether astrocytic signaling contribute to MMN responses in A1 is currently unknown.

Recent studies emphasize the importance of whole-brain connectivity for processing auditory stimuli. In particular, the frontal cortex is known to play a central role on top-down control of sound prediction errors[4]. The PPC, a critical hub for multisensory integration[59] and higher-order auditory processing[5,6], was known to respond to unexpected sounds[7-9]; however, its precise role in differentiating redundant from deviant auditory stimuli remained unclear. In this study, we showed that while PPC exhibited a strong response to both unexpected and deviant sounds, its response to repetitive sounds was negligible. Notably, ketamine administration did not affect the N1 component, while it abolished the P1 component of MMN, which is thought to carry the novelty content of the response. We thus chose the late response's period to perform further connectivity analysis. By using both Granger causality and WPLI analysis, we provided, to the best of our knowledge, the first evidence of A1 to PPC functional connectivity during deviance detection. We further showed that this process is dependent on intact NMDA signaling. Ketamine administration may affect primarily A1 responses, in turn abolishing the functional connectivity from A1 to PPC, or/and it may directly affect PPC local circuits. Nevertheless, our data is consistent with previous studies reporting a decrease in directed functional connectivity for different psychedelics, including subanesthetic ketamine, throughout the brain[60,61]. These data further support the hypothesis that the psychedelic state involves a breakdown in patterns of functional organization or information flow in the brain[60].

Somewhat contradictory, ketamine's ability to restore impaired cortical networks, particularly in regions such as the prefrontal cortex, is considered central to its antidepressant effects [62,63,64,65]. This may be due to the specific nature of the underlying pathophysiology of treatment-resistant depression. MMN has been shown to be impaired in psychiatric disorders such as depression [66] and schizophrenia [67], both of which have been linked to NMDA receptor

dysfunction, although in opposite directions. In schizophrenia, NMDA receptor hypofunction is thought to contribute to reduced MMN amplitude and sensory processing deficits, while in depression, NMDA receptor hyperfunction is believed to underlie similar sensory processing disruptions[68-70]. Although, the therapeutic mechanisms behind ketamine's anti-depressive effects are still not well understood, they are thought to involve multiple parallels mechanisms, including altered neurotransmission through NMDA receptor antagonism, but also enhanced synaptic plasticity and modulation of various signaling pathways, including the mTOR pathway [71].

In summary, our data identified a specific biphasic spiking response in a subpopulation of A1 neurons elicited by deviant, but not standard, sounds, whereby the second peak is dependent upon NMDA receptor-mediated signaling. The identity of the neurons participating to this response and the underlying microcircuit mechanisms remain to be elucidated. We further provided evidence that PPC responds to unexpected and deviant, but not repetitive, sounds, and that this response is NMDA receptor-dependent. Finally, we showed a unidirectional functional connectivity from A1 to PPC during deviant detection, which is abolished by subanesthetic ketamine administration. Together, these data support the hypothesis that PPC plays a role, dependent upon intact NMDA receptor-mediated signaling, in prediction error.

ACKNOWLEDGEMENTS

We would like to thank Kristian Agbogba, Mikael Valton Charette and James Waldron for their technical assistance, the Comité Institutionnel de Bonne Pratiques Animales en Recherche (CIBPAR), all the personnel of the animal facility of the Research Center of CHU Sainte-Justine (Université de Montreal) and Compute Canada for their instrumental technical support and members of our lab for insightful data discussion. We would also like to thank Dr Jozsef Csicsvari for sharing their spike sorting analysis pipeline. This work was supported by the Natural Sciences and Engineering Research Council of Canada (NSERC) and La Fondation des Étoiles (G.DC.). M.I.C-M and A.C.C are supported

by the Canadian Neurodevelopmental Research Training (CanNRT) Platform. M.I.C-M is supported by Savoy Foundation fellowship.

REFERENCES

1 Harms, L., Michie, P. T. & Naatanen, R. Criteria for determining whether mismatch responses exist in animal models: Focus on rodents. *Biol Psychol* **116**, 28-35, doi:10.1016/j.biopsycho.2015.07.006 (2016).

2 Rosburg, T. & Mager, R. The reduced auditory evoked potential component N1 after repeated stimulation: Refractoriness hypothesis vs. habituation account. *Hear Res* **400**, 108140, doi:10.1016/j.heares.2020.108140 (2021).

3 Naatanen, R., Paavilainen, P., Rinne, T. & Alho, K. The mismatch negativity (MMN) in basic research of central auditory processing: a review. *Clin Neurophysiol* **118**, 2544-2590, doi:10.1016/j.clinph.2007.04.026 (2007).

4 Hockley, A., Bohorquez, L. H. & Malmierca, M. S. Top-down prediction signals from the medial prefrontal cortex govern auditory cortex prediction errors. *Cell Rep* **44**, 115538, doi:10.1016/j.celrep.2025.115538 (2025).

5 Andersen, R. A. & Buneo, C. A. Intentional maps in posterior parietal cortex. *Annu Rev Neurosci* **25**, 189-220, doi:10.1146/annurev.neuro.25.112701.142922 (2002).

6 Van Derveer, A. B., Ross, J. M. & Hamm, J. P. Robust multisensory deviance detection in the mouse parietal associative area. *Curr Biol* **33**, 3969-3976 e3964, doi:10.1016/j.cub.2023.08.002 (2023).

7 Justen, C. & Herbert, C. The spatio-temporal dynamics of deviance and target detection in the passive and active auditory oddball paradigm: a sLORETA study. *BMC Neurosci* **19**, 25, doi:10.1186/s12868-018-0422-3 (2018).

8 Raltschev, C., Kasavica, S., Leonardon, B., Nevian, T. & Sachidhanandam, S. Top-down modulation of sensory processing and mismatch in the mouse posterior parietal cortex. *Nat Commun* **16**, 4240, doi:10.1038/s41467-025-58002-2 (2025).

9 Mohan, H. *et al.* Sensory representation of an auditory cued tactile stimulus in the posterior parietal cortex of the mouse. *Sci Rep* **8**, 7739, doi:10.1038/s41598-018-25891-x (2018).

10 Rosburg, T. & Kreitschmann-Andermahr, I. The effects of ketamine on the mismatch negativity (MMN) in humans - A meta-analysis. *Clin Neurophysiol* **127**, 1387-1394, doi:10.1016/j.clinph.2015.10.062 (2016).

11 Light, G. A. & Naatanen, R. Mismatch negativity is a breakthrough biomarker for understanding and treating psychotic disorders. *Proc Natl Acad Sci U S A* **110**, 15175-15176, doi:10.1073/pnas.1313287110 (2013).

12 Kreitschmann-Andermahr, I. *et al.* Effect of ketamine on the neuromagnetic mismatch field in healthy humans. *Brain Res Cogn Brain Res* **12**, 109-116, doi:10.1016/s0926-6410(01)00043-x (2001).

13 Umbricht, D. *et al.* Ketamine-induced deficits in auditory and visual context-dependent processing in healthy volunteers: implications for models of cognitive deficits in schizophrenia. *Arch Gen Psychiatry* **57**, 1139-1147, doi:10.1001/archpsyc.57.12.1139 (2000).

14 Thiebes, S. *et al.* Glutamatergic deficit and schizophrenia-like negative symptoms: new evidence from ketamine-induced mismatch negativity alterations in healthy male humans. *J Psychiatry Neurosci* **42**, 273-283, doi:10.1503/jpn.160187 (2017).
15 Umbricht, D. & Krljes, S. Mismatch negativity in schizophrenia: a meta-analysis. *Schizophr Res* **76**, 1-23, doi:10.1016/j.schres.2004.12.002 (2005).
16 McLean, A. C., Valenzuela, N., Fai, S. & Bennett, S. A. Performing vaginal lavage, crystal violet staining, and vaginal cytological evaluation for mouse estrous cycle staging identification. *J Vis Exp*, e4389, doi:10.3791/4389 (2012).
17 Carreno-Munoz, M. I. *et al.* Sensory processing dysregulations as reliable translational biomarkers in SYNGAP1 haploinsufficiency. *Brain* **145**, 754-769, doi:10.1093/brain/awab329 (2022).
18 Oostenveld, R., Fries, P., Maris, E. & Schoffelen, J. M. FieldTrip: Open source software for advanced analysis of MEG, EEG, and invasive electrophysiological data. *Comput Intell Neurosci* **2011**, 156869, doi:10.1155/2011/156869 (2011).
19 Harris, K. D., Henze, D. A., Csicsvari, J., Hirase, H. & Buzsaki, G. Accuracy of tetrode spike separation as determined by simultaneous intracellular and extracellular measurements. *J Neurophysiol* **84**, 401-414, doi:10.1152/jn.2000.84.1.401 (2000).
20 Csicsvari, J., Hirase, H., Czurko, A. & Buzsaki, G. Reliability and state dependence of pyramidal cell-interneuron synapses in the hippocampus: an ensemble approach in the behaving rat. *Neuron* **21**, 179-189, doi:10.1016/s0896-6273(00)80525-5 (1998).
21 Gil-da-Costa, R., Stoner, G. R., Fung, R. & Albright, T. D. Nonhuman primate model of schizophrenia using a noninvasive EEG method. *Proc Natl Acad Sci U S A* **110**, 15425-15430, doi:10.1073/pnas.1312264110 (2013).
22 Schuelert, N., Dorner-Ciossek, C., Brendel, M. & Rosenbrock, H. A comprehensive analysis of auditory event-related potentials and network oscillations in an NMDA receptor antagonist mouse model using a novel wireless recording technology. *Physiol Rep* **6**, e13782, doi:10.14814/phy2.13782 (2018).
23 Picard, N., Takesian, A. E., Fagiolini, M. & Hensch, T. K. NMDA 2A receptors in parvalbumin cells mediate sex-specific rapid ketamine response on cortical activity. *Mol Psychiatry* **24**, 828-838, doi:10.1038/s41380-018-0341-9 (2019).
24 Ehrlichman, R. S., Maxwell, C. R., Majumdar, S. & Siegel, S. J. Deviance-elicited changes in event-related potentials are attenuated by ketamine in mice. *J Cogn Neurosci* **20**, 1403-1414, doi:10.1162/jocn.2008.20097 (2008).
25 de la Salle, S. *et al.* N-methyl-D-aspartate receptor antagonism impairs sensory gating in the auditory cortex in response to speech stimuli. *Psychopharmacology (Berl)* **239**, 2155-2169, doi:10.1007/s00213-022-06090-z (2022).
26 Bigelow, J., Morrill, R. J., Dekloe, J. & Hasenstaub, A. R. Movement and VIP Interneuron Activation Differentially Modulate Encoding in Mouse Auditory Cortex. *eNeuro* **6**, doi:10.1523/ENEURO.0164-19.2019 (2019).
27 Schneider, D. M., Nelson, A. & Mooney, R. A synaptic and circuit basis for corollary discharge in the auditory cortex. *Nature* **513**, 189-194, doi:10.1038/nature13724 (2014).
28 Chen, I. W., Helmchen, F. & Lutcke, H. Specific Early and Late Oddball-Evoked Responses in Excitatory and Inhibitory Neurons of Mouse Auditory Cortex. *J Neurosci* **35**, 12560-12573, doi:10.1523/JNEUROSCI.2240-15.2015 (2015).
29 Ulanovsky, N., Las, L. & Nelken, I. Processing of low-probability sounds by cortical neurons. *Nat Neurosci* **6**, 391-398, doi:10.1038/nn1032 (2003).

30 Mikell, C. B. *et al.* Features and timing of the response of single neurons to novelty in the substantia nigra. *Brain Res* **1542**, 79-84, doi:10.1016/j.brainres.2013.10.033 (2014).
31 Camalier, C. R., Scarim, K., Mishkin, M. & Averbeck, B. B. A Comparison of Auditory Oddball Responses in Dorsolateral Prefrontal Cortex, Basolateral Amygdala, and Auditory Cortex of Macaque. *J Cogn Neurosci* **31**, 1054-1064, doi:10.1162/jocn_a_01387 (2019).
32 Mulert, C. *et al.* Auditory cortex and anterior cingulate cortex sources of the early evoked gamma-band response: relationship to task difficulty and mental effort. *Neuropsychologia* **45**, 2294-2306, doi:10.1016/j.neuropsychologia.2007.02.020 (2007).
33 Polomac, N. *et al.* Generators and Connectivity of the Early Auditory Evoked Gamma Band Response. *Brain Topogr* **28**, 865-878, doi:10.1007/s10548-015-0434-6 (2015).
34 Lee, M. *et al.* Rodent Mismatch Negativity/theta Neuro-Oscillatory Response as a Translational Neurophysiological Biomarker for N-Methyl-D-Aspartate Receptor-Based New Treatment Development in Schizophrenia. *Neuropsychopharmacology* **43**, 571-582, doi:10.1038/npp.2017.176 (2018).
35 Curic, S. *et al.* Reduced auditory evoked gamma-band response and schizophrenia-like clinical symptoms under subanesthetic ketamine. *Neuropsychopharmacology* **44**, 1239-1246, doi:10.1038/s41386-019-0328-5 (2019).
36 Bastos, A. M. & Schoffelen, J. M. A Tutorial Review of Functional Connectivity Analysis Methods and Their Interpretational Pitfalls. *Front Syst Neurosci* **9**, 175, doi:10.3389/fnsys.2015.00175 (2015).
37 Vinck, M., Oostenveld, R., van Wingerden, M., Battaglia, F. & Pennartz, C. M. An improved index of phase-synchronization for electrophysiological data in the presence of volume-conduction, noise and sample-size bias. *Neuroimage* **55**, 1548-1565, doi:10.1016/j.neuroimage.2011.01.055 (2011).
38 Fitzgerald, K. & Todd, J. Making Sense of Mismatch Negativity. *Front Psychiatry* **11**, 468, doi:10.3389/fpsyt.2020.00468 (2020).
39 Javitt, D. C. & Sweet, R. A. Auditory dysfunction in schizophrenia: integrating clinical and basic features. *Nat Rev Neurosci* **16**, 535-550, doi:10.1038/nrn4002 (2015).
40 Homayoun, H. & Moghaddam, B. NMDA receptor hypofunction produces opposite effects on prefrontal cortex interneurons and pyramidal neurons. *J Neurosci* **27**, 11496-11500, doi:10.1523/JNEUROSCI.2213-07.2007 (2007).
41 Grunze, H. C. *et al.* NMDA-dependent modulation of CA1 local circuit inhibition. *J Neurosci* **16**, 2034-2043, doi:10.1523/JNEUROSCI.16-06-02034.1996 (1996).
42 Middleton, S. *et al.* NMDA receptor-dependent switching between different gamma rhythm-generating microcircuits in entorhinal cortex. *Proc Natl Acad Sci U S A* **105**, 18572-18577, doi:10.1073/pnas.0809302105 (2008).
43 Li, Q., Clark, S., Lewis, D. V. & Wilson, W. A. NMDA receptor antagonists disinhibit rat posterior cingulate and retrosplenial cortices: a potential mechanism of neurotoxicity. *J Neurosci* **22**, 3070-3080, doi:10.1523/JNEUROSCI.22-08-03070.2002 (2002).
44 Widman, A. J. & McMahon, L. L. Disinhibition of CA1 pyramidal cells by low-dose ketamine and other antagonists with rapid antidepressant efficacy. *Proc Natl Acad Sci U S A* **115**, E3007-E3016, doi:10.1073/pnas.1718883115 (2018).

45 Buzsaki, G. & Wang, X. J. Mechanisms of gamma oscillations. *Annu Rev Neurosci* **35**, 203-225, doi:10.1146/annurev-neuro-062111-150444 (2012).
46 Cho, K. K. A., Shi, J., Phensy, A. J., Turner, M. L. & Sohal, V. S. Long-range inhibition synchronizes and updates prefrontal task activity. *Nature* **617**, 548-554, doi:10.1038/s41586-023-06012-9 (2023).
47 Zurita, H., Feyen, P. L. C. & Apicella, A. J. Layer 5 Callosal Parvalbumin-Expressing Neurons: A Distinct Functional Group of GABAergic Neurons. *Front Cell Neurosci* **12**, 53, doi:10.3389/fncel.2018.00053 (2018).
48 Kullander, K. & Topolnik, L. Cortical disinhibitory circuits: cell types, connectivity and function. *Trends Neurosci* **44**, 643-657, doi:10.1016/j.tins.2021.04.009 (2021).
49 Kim, S. H., Price, M. T., Olney, J. W. & Farber, N. B. Excessive cerebrocortical release of acetylcholine induced by NMDA antagonists is reduced by GABAergic and alpha2-adrenergic agonists. *Mol Psychiatry* **4**, 344-352, doi:10.1038/sj.mp.4000529 (1999).
50 Kikuchi, T., Wang, Y., Shinbori, H., Sato, K. & Okumura, F. Effects of ketamine and pentobarbitone on acetylcholine release from the rat frontal cortex in vivo. *Br J Anaesth* **79**, 128-130, doi:10.1093/bja/79.1.128 (1997).
51 Harkrider, A. W. & Hedrick, M. S. Acute effect of nicotine on auditory gating in smokers and non-smokers. *Hear Res* **202**, 114-128, doi:10.1016/j.heares.2004.11.009 (2005).
52 Inami, R., Kirino, E., Inoue, R. & Arai, H. Transdermal nicotine administration enhances automatic auditory processing reflected by mismatch negativity. *Pharmacol Biochem Behav* **80**, 453-461, doi:10.1016/j.pbb.2005.01.001 (2005).
53 Inami, R., Kirino, E., Inoue, R., Suzuki, T. & Arai, H. Nicotine effects on mismatch negativity in nonsmoking schizophrenic patients. *Neuropsychobiology* **56**, 64-72, doi:10.1159/000111536 (2007).
54 Martin, L. F., Davalos, D. B. & Kisley, M. A. Nicotine enhances automatic temporal processing as measured by the mismatch negativity waveform. *Nicotine Tob Res* **11**, 698-706, doi:10.1093/ntr/ntp052 (2009).
55 Hamilton, H. K. *et al.* Interactive effects of an N-methyl-d-aspartate receptor antagonist and a nicotinic acetylcholine receptor agonist on mismatch negativity: Implications for schizophrenia. *Schizophr Res* **191**, 87-94, doi:10.1016/j.schres.2017.06.040 (2018).
56 Weber, L. A. *et al.* Auditory mismatch responses are differentially sensitive to changes in muscarinic acetylcholine versus dopamine receptor function. *Elife* **11**, doi:10.7554/eLife.74835 (2022).
57 Xin, Q. *et al.* Neuron-astrocyte coupling in lateral habenula mediates depressive-like behaviors. *Cell* **188**, 3291-3309 e3224, doi:10.1016/j.cell.2025.04.010 (2025).
58 Lefton, K. B. *et al.* Norepinephrine signals through astrocytes to modulate synapses. *Science* **388**, 776-783, doi:10.1126/science.adq5480 (2025).
59 Choi, I. & Lee, S. H. Locomotion-dependent auditory gating to the parietal cortex guides multisensory decisions. *Nat Commun* **16**, 2308, doi:10.1038/s41467-025-57347-y (2025).
60 Barnett, L., Muthukumaraswamy, S. D., Carhart-Harris, R. L. & Seth, A. K. Decreased directed functional connectivity in the psychedelic state. *Neuroimage* **209**, 116462, doi:10.1016/j.neuroimage.2019.116462 (2020).

61 Muthukumaraswamy, S. D. *et al.* Evidence that Subanesthetic Doses of Ketamine Cause Sustained Disruptions of NMDA and AMPA-Mediated Frontoparietal Connectivity in Humans. *J Neurosci* **35**, 11694-11706, doi:10.1523/JNEUROSCI.0903-15.2015 (2015).
62 Li, C. T. *et al.* The effects of low-dose ketamine on the prefrontal cortex and amygdala in treatment-resistant depression: A randomized controlled study. *Hum Brain Mapp* **37**, 1080-1090, doi:10.1002/hbm.23085 (2016).
63 Roussy, M. *et al.* Ketamine disrupts naturalistic coding of working memory in primate lateral prefrontal cortex networks. *Mol Psychiatry* **26**, 6688-6703, doi:10.1038/s41380-021-01082-5 (2021).
64 Abdallah, C. G. *et al.* Ketamine Treatment and Global Brain Connectivity in Major Depression. *Neuropsychopharmacology* **42**, 1210-1219, doi:10.1038/npp.2016.186 (2017).
65 Gass, N. *et al.* Differences between ketamine's short-term and long-term effects on brain circuitry in depression. *Transl Psychiatry* **9**, 172, doi:10.1038/s41398-019-0506-6 (2019).
66 Tseng, Y. J., Nouchi, R. & Cheng, C. H. Mismatch negativity in patients with major depressive disorder: A meta-analysis. *Clin Neurophysiol* **132**, 2654-2665, doi:10.1016/j.clinph.2021.06.019 (2021).
67 Molnar, H. *et al.* A comparison of visual and acoustic mismatch negativity as potential biomarkers in schizophrenia. *Sci Rep* **14**, 992, doi:10.1038/s41598-023-49983-5 (2024).
68 Wang, S., Bian, L., Yin, Y. & Guo, J. Targeting NMDA Receptors in Emotional Disorders: Their Role in Neuroprotection. *Brain Sci* **12**, doi:10.3390/brainsci12101329 (2022).
69 Adell, A. Brain NMDA Receptors in Schizophrenia and Depression. *Biomolecules* **10**, doi:10.3390/biom10060947 (2020).
70 Balu, D. T. The NMDA Receptor and Schizophrenia: From Pathophysiology to Treatment. *Adv Pharmacol* **76**, 351-382, doi:10.1016/bs.apha.2016.01.006 (2016).
71 Duman, R. S., Aghajanian, G. K., Sanacora, G. & Krystal, J. H. Synaptic plasticity and depression: new insights from stress and rapid-acting antidepressants. *Nat Med* **22**, 238-249, doi:10.1038/nm.4050 (2016).

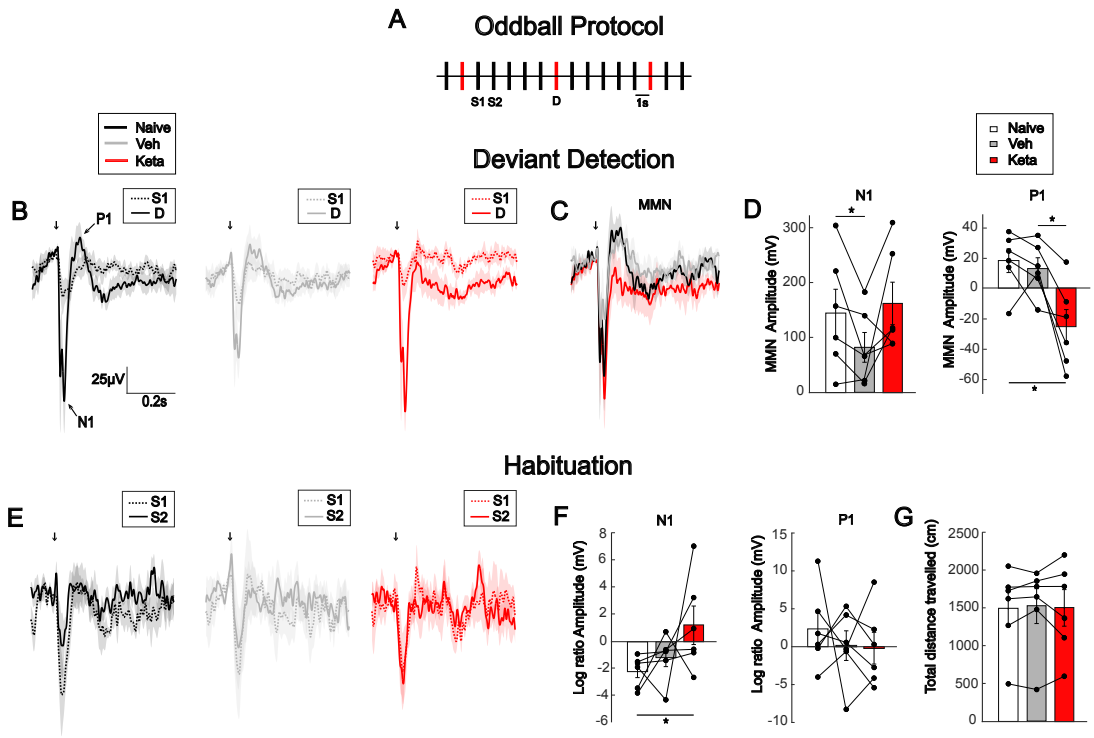

Figure 1. Subanesthetic ketamine alters MMN responses during deviant detection and stimulus specific adaption. (**A**) Schematic representation of the oddball protocol with black bars representing 5kHz pure tones (standard sounds) and the red bars 10kHz pure tones (deviant sounds). (**B**) Mean AEP (auditory evoked potentials) traces of standard (dotted) and deviant (solid) sounds for naive (left), vehicle injected (middle), and low-dose ketamine injected (right) mice. Arrows indicate the start time of stimulation. N1 is identified as the first negative peak ~10-20 ms and P1 as the first positive peak ~30-40 ms. (**C**) Superposed MMN (deviant—standard) traces. (**D**) Bar plots of MMN N1 (Naive-Keta Wilcoxon signed ranked test; z =0.314, p =0.753; Naive-Veh Wilcoxon signed ranked test; z =-1.992, p =0.046; Veh-Keta Wilcoxon signed ranked test; z =1.572, p =0.116) and MMN P1 (Ctrl-Keta Wilcoxon signed ranked test: z=-2.201, p=0.028; Naive-Veh Wilcoxon signed ranked test; z =-0.943, p =0.345; Veh-Keta Wilcoxon signed ranked test: z=2.201, p=0.028) peak amplitude. (**E**) Mean response to the first (dotted) and second (solid) standard sound for naive (left), vehicle injected (middle), and low-dose ketamine injected (right) mice. (**F**) Bar plots show N1(Naive-Keta Wilcoxon signed ranked test; z =1.572, p=0.116; Naive-Veh Wilcoxon signed ranked test; z =1.363, p=0.173; Veh-Keta Wilcoxon signed ranked test; z =1.153, p=0.249) and P1(Ctrl-Keta Wilcoxon signed ranked test; z =-0.524, p=0.600; Naive-Veh Wilcoxon signed ranked test; z =-0.105, p=0.917; Veh-Keta Wilcoxon signed ranked test; z =-0.314, p=0.753) amplitude after first (S1) versus second (S2) sounds in mice. (**G**) Bar plot of total distance travelled (Ctrl-Keta Wilcoxon signed ranked test; z =0.105, p =0.917; Naive-Veh Wilcoxon signed ranked test; z =0.734, p=0.463; Veh-Keta Wilcoxon signed ranked test; z =-0.105, p=0.917). Naïve mice, n = 6; Vehicle-injected mice, n = 6; Ketamine-injected mice, n = 6.

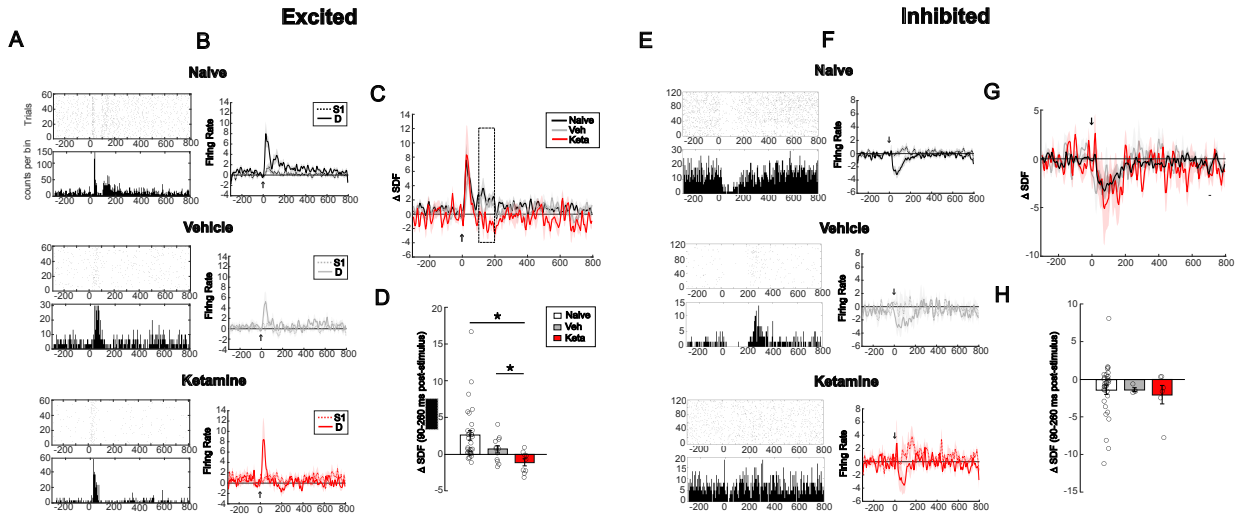

Figure 2. Subanesthetic ketamine alters spiking activity of responding neurons during deviant detection and stimulus specific adaptation. (**A**, **E**) Raster plots (top) and PTSH (bottom) for representative responding excited (**A**) and inhibited (**E**) neurons in naïve (top-black), vehicle injected (middle-gray), and ketamine injected (bottom-red) mice. (**B**, **F**) Firing probability of responding excited (**B**) and inhibited (**F**) neurons in each condition. (**C**, **G**) Spike density function of the MMN of responding excited (**C**) and responding inhibited (**G**) neurons in naive (top), vehicle injected (middle), and ketamine injected (bottom) mice. (**D**, **H**) Bar plots of MMN evoked firing responses of responding excited cells (**D**; Naive-Keta Linear mixed model: p= 0.034, mean difference= 2.950, std. error=1.346; Naive-Veh Linear mixed model: p= 0.029, mean difference= 1.549, std.error=0.658; Veh-Keta Linear mixed model: p=0.323, mean difference=-1.18, std.error=1.18)) and responding inhibited cells (**H**; Naive-Keta Linear mixed model: p= 0.660, mean difference= 0.584, std. error=1.317; Naive-Veh Linear mixed model: p= 0.791, mean difference=0.383, std.error=1.432; Veh-Keta Linear mixed model: p=0.639, mean difference=0.674, std.error=1.384)). Responding excited neurons: n=36 cells from 5 mice (naïve), n=12 cells from 4 mice (vehicle-injected), and n= 9 cells from 5 mice (ketamine-injected). Responding inhibited neurons: n=33 cells from 5 mice (naive), n=4 cells from 2 mice (vehicle-injected), and n= 6 cells from 4 mice (ketamine-injected.

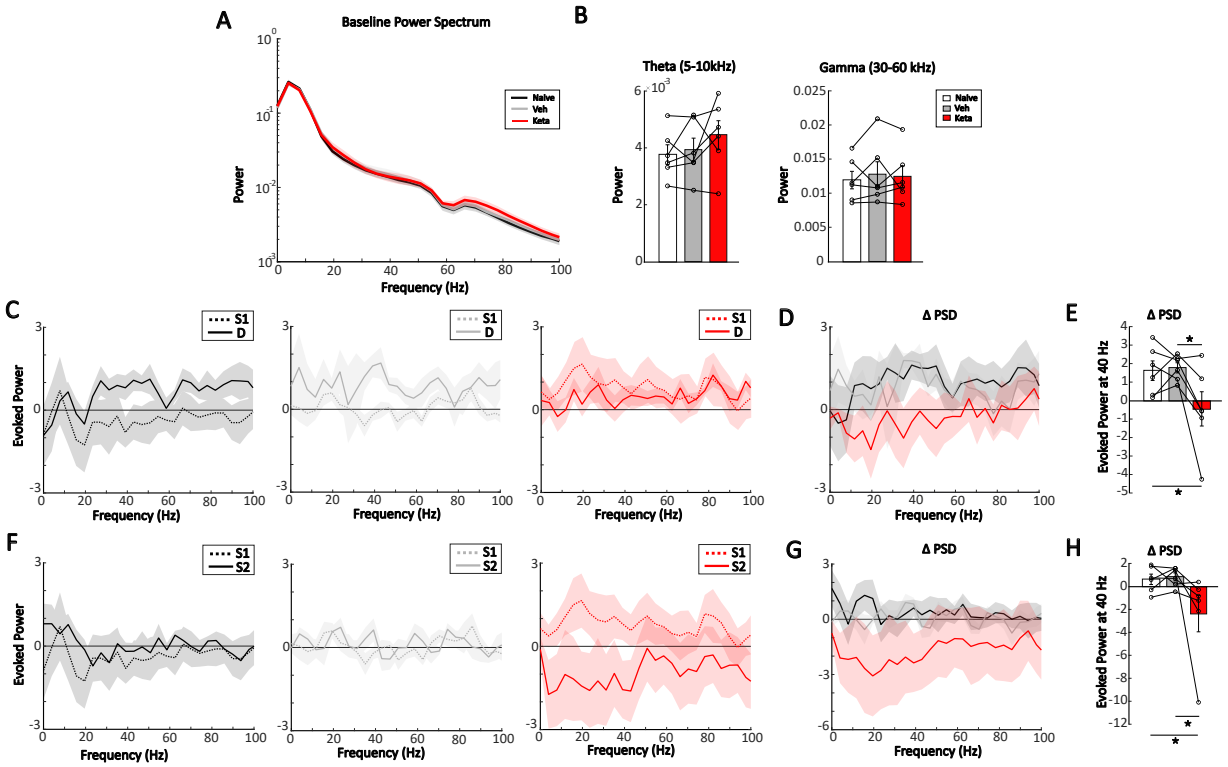

Figure 3. Subanesthetic ketamine affects power density spectra during deviance detection. (**A**) Power density spectra (5–100Hz) of 3-min baseline state (non-stimulus) EEG signal from the auditory cortex. (**B**) Bar plots show mean powers ± SEM of the theta (Naive- Keta Wilcoxon signed ranked test: z= 0.524, p=0.600; Veh-Keta Wilcoxon signed ranked test: z=-0.105, p=0.917; Ctrl-Veh Wilcoxon signed ranked test: z=0.943, p=0.345) and gamma (Naive- Keta Wilcoxon signed ranked test: z= 1.572, p=0.116; Veh-Keta Wilcoxon signed ranked test: z=0.943, p=0.345; Ctrl-Veh Wilcoxon signed ranked test: z=0.524, p=0.600) bands in mice. (**C**) Evoked power in response to standard and deviant sounds in naive (left), vehicle-injected (middle), and ketamine-injected (right) mice. (**D**) MMN of evoked power in response to standard and deviant sounds across all frequencies. (**E**) Bar plot of MMN of evoked power at 40 Hz (Naive- Keta Wilcoxon signed ranked test: z= -2.201, p=0.028; Veh-Keta Wilcoxon signed ranked test: z=1.992, p=0.046; Naive-Veh Wilcoxon signed ranked test: z=-0.524, p=0.600). (**F**) Evoked power in response to the first (S1) and second (S2) standard sounds in naive (left), vehicle-injected (middle), and ketamine-injected (right) mice. (**G**) Evoked power of the log ratio of the second and first standard sounds across all frequencies (S2/S1). (**H**) Bar plot of S2/S1 log ratio evoked power at 40 Hz (Naive-Keta Wilcoxon signed ranked test: z= -2.201, p=0.028; Veh-Keta Wilcoxon signed ranked test: z=1.992, p=0.046; Naïve-Veh Wilcoxon signed ranked test: z=0.524, p=0.600). Naïve mice, n = 6; Vehicle-injectes mice, n = 6; Ketamine-injected mice, n = 6.

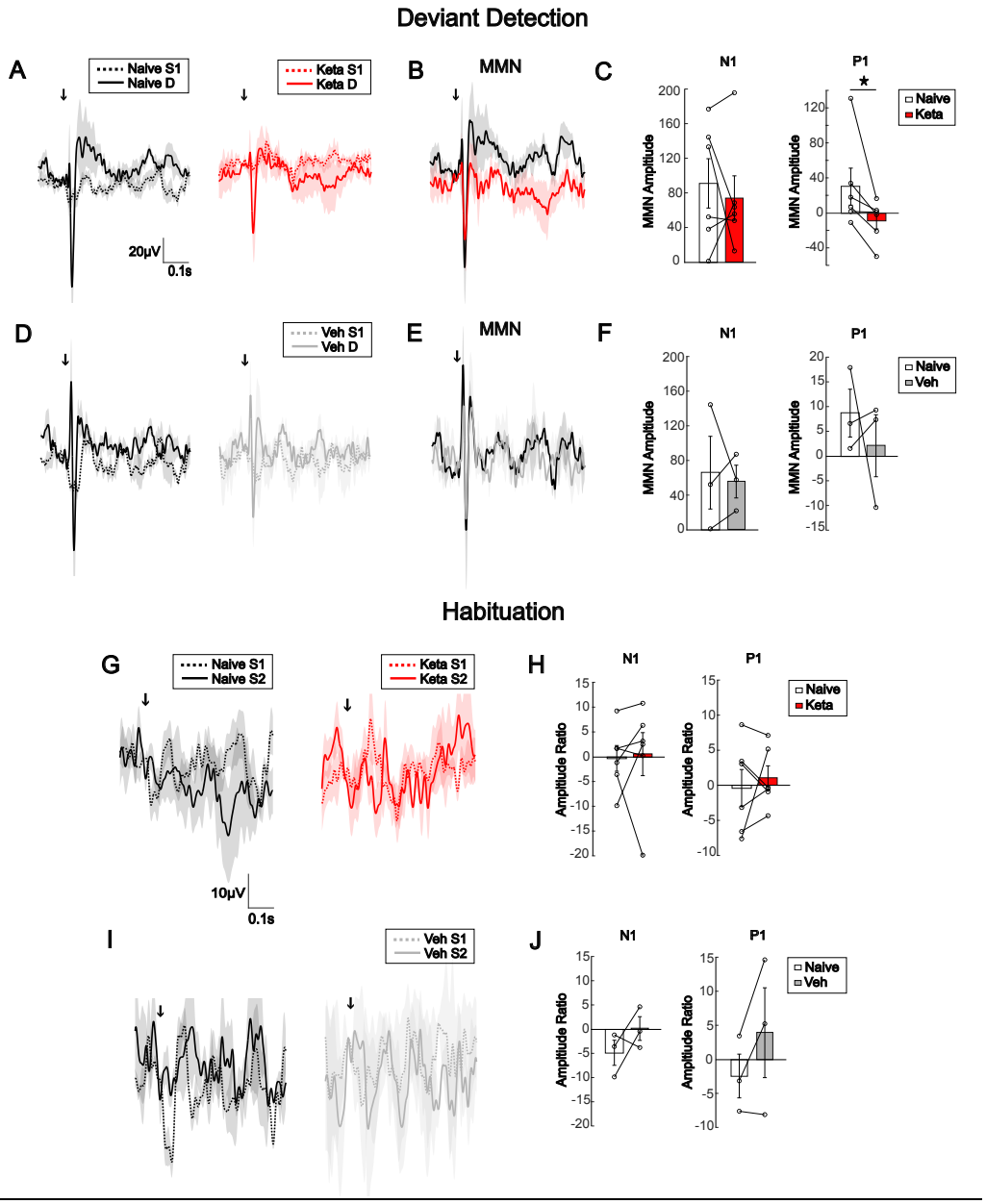

Figure 4. PPC encodes deviance detection. (**A**, **B**) Deviant detection in the PPC of naive vs ketamine injected mice. (**A**) Mean AEP traces of standard (dotted) and deviant (solid) sounds for naive (left) versus low-dose ketamine injected (right) mice. (**B**) Superposed MMN (deviant—standard) traces. (**C**) Bar plots of MMN N1 (Wilcoxon signed ranked test: z=-0.314, p=0.753) and MMN P1 (Wilcoxon signed ranked test: z=-2.201, p=0.028) peak amplitude in naive and ketamine-injected mice. (**D-F**) Deviant detection in the PPC of naive vs vehicle-injected mice. (**D**) Mean AEP traces of standard (dotted) and deviant (solid) sounds for naive (left) and vehicle injected (right) mice. (**E**) Superposed MMN (deviant—standard) traces. (**F**) Bar plots of MMN N1 (Wilcoxon signed ranked test: z=-2.201, p=0.028) and MMN P1(Wilcoxon signed ranked test: z=0.0, p=1.00). (**G**) Mean AEP traces of the first (dotted) and second (solid) standard sounds for naïve (left) versus ketamine-injected (right) mice. (**H**) Bar plots of S2/S1 log ratio N1(Wilcoxon

signed ranked test: z=0.524, p=0.600) and P1 (Wilcoxon signed ranked test: z=105, p=0.917) peak amplitude in naive and ketamine-injected mice. (**I**) Mean AEP traces of the first (dotted) and second (solid) standard sounds for naive (left) versus vehicle injected (right) mice. (J) Bar plots of S2/S1 log ratio N1(Wilcoxon signed ranked test: z=1.069, p=0.285) and P1 (Wilcoxon signed ranked test: z=1.069, p=0.285) peak amplitude in naive and ketamine-injected mice. Naive (n=6) versus Ketamine-injected (n=6) mice; naive(n=3) versus Vehicle-injected (n=3) mice.

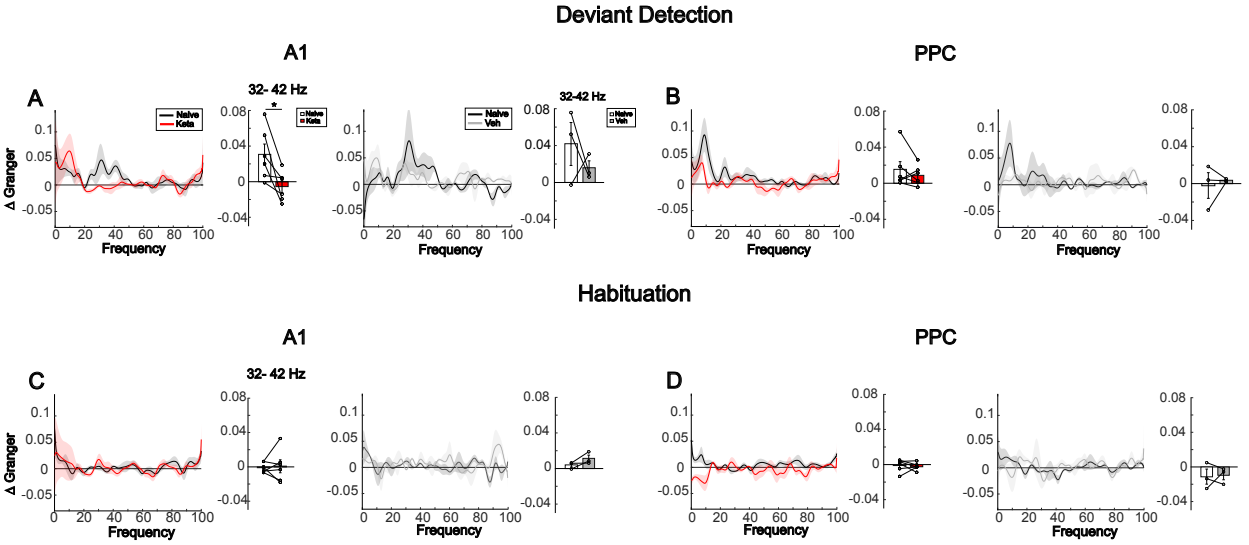

Figure 5. Subanesthetic ketamine decreases predictive connectivity from A1 to PPC. (A, B) Granger causality during deviant detection. Granger causality of MMN (deviant-standard) (left) and bar plot of their Granger index at 32-42 Hz (right) from A1 to PPC (**A**) and from PPC to A1 (**B**) for naive versus ketamine-injected mice (left) (Wilcoxon signed ranked test: z= -2.201, p=0.028) and naive versus vehicle-injected mice (right) (Wilcoxon signed ranked test: z= -1.069 9, p=0.285) mice. (**C**, **D**) Granger causality during auditory habituation. Granger causality of the log ratio of the second and first standard sounds (S2/S1) and bar plot of their Granger index at 32-42 Hz from A1 to PPC (**C**) and from PPC to A1 (**D**) for naive versus ketamine-injected mice (left) (Wilcoxon signed ranked test: z= -0.734, p=0.463) and Naive versus vehicle-injected mice (right) (Wilcoxon signed ranked test: z= 0.00, p=1.00) mice. Naive (n=6) versus Ketamine-injected (n=6) mice; naive (n=3) versus Vehicle-injected (n=3) mice.